IEEE Access
Multidisciplinary ⋮ Rapid Review ⋮ Open Access Journal

Received March 9, 2020, accepted March 27, 2020, date of publication April 6, 2020, date of current version April 24, 2020.

Digital Object Identifier 10.1109/ACCESS.2020.2985992

Study of a Multi-Loop Travelling Wave UHF RFID Near-Field Antenna

ZIJIAN XING[1], HAOTIAN LI[1], CHOW-YEN-DESMOND SIM[2], (Senior Member, IEEE), JIANYING LI[1], AND ZILIANG LI[1]

[1]School of Electronics and Information Engineering, Northwestern Polytechnical University, Xi'an 710072, China
[2]Department of Electrical Engineering, Feng Chia University, Taichung 40724, Taiwan

Corresponding author: Zijian Xing (xingzijian2004@126.com)

This work was supported in part by the National Natural Science Foundation of China under Grant 61601373, Grant 61701414, and Grant 61871324, in part by the Aerospace Science and Technology Innovation Fund of China under Grant 2016KC080013, and in part by the Central University Fundamental Research Fund of China under Grant G2019KY05204.

ABSTRACT A multi-loop travelling-wave ultra-high frequency (UHF) radio frequency identification (RFID) near-field antenna (NFA) is proposed and investigated. To achieve strong and uniform magnetic field, as well as extendable reading range, multiple λ/2 rectangular loop structures printed on both sides of an FR4 substrate is adopted. Via the RFID system measurement for magnetic field distribution, the maximum reading range of the proposed NFA is 11 cm, and its corresponding 100% reading rate distance is 5 cm. Here, broad 10-dB impedance bandwidth of 18.7% (816–984 MHz) was measured, which can cover both ETSI (European Telecommunication Standards Institute) and FCC (Federal Communications Commission) bands. Parametric studies are further carried out to facilitate the design and optimization processes.

INDEX TERMS UHF RFID, near-field antenna, travelling wave, multiple loop.

I. INTRODUCTION

Radio frequency identification (RFID) has been a widely used non-contact automatic recognition technology for wireless identification and tracking ability. Typical RFID system includes reader, tag and post-processing system, and it is conventionally divided into far-field system (FFS) and near-field system (NFS) based on operating distance [1]. For NFS that operates in the ultra-high frequency (UHF), it can provide higher data-rate and read-rate than those in high frequency (HF) or low frequency (LF) [2]. In addition, HF and LF antennas are mostly multi-turn loop structures because of long wavelength. In contrast, the antenna wavelength in the UHF band is much smaller. Because the reader antenna can directly affect the system operating distance, research and development for UHF RFID near-field applications in recent years have been focusing on its NFA designs, in which the near-field inductive coupling type is commonly used [3]. Here, it is noteworthy that the near-field inductive coupling systems are rarely affected by adjacent metal or liquid, and is only affected by objects with high magnetic permeability. For inductive coupling, the energy is mainly stored in the form of magnetic field, which requires the reader antenna to produce strong and uniform magnetic field in the near field zone. Different from the traditional miniaturization of the antenna, one of the pursuits of the UHF near field RFID reader antenna is to have a large size, as it is the basis for obtaining a large planar reading range.

NFA for near-field UHF RFID applications can be divided into three types, namely, loop antenna, oppositely directed currents (ODCs) structure antenna and travelling-wave antenna. For loop antenna, it is impractical to directly adopt conventional solid-line loop structure, because at UHF band such structure in target area will always produce reverse currents, thus greatly weaken the magnetic field intensity and adversely affect the field uniformity. Here, one typical method to eliminate the reverse currents is to adopt segmented line structure [4]–[11], and the other method is to insert components such as capacitances [12] and phase-shifter stubs [13], so that the incurred phase delay can be compensated. To form electrically large loops, dipole structure designs have also been reported in [14], [15]. For ODCs structure antenna, the design is based on the phenomenon that the magnetic field intensity is added up when the currents on two adjacent lines flow in the opposite direction [16]. Therefore, it is common to adopt dipoles generating in-phase current and magnetic field distribution [17]–[19]. For travelling-wave antenna design [20]–[25], there always exist

The associate editor coordinating the review of this manuscript and approving it for publication was Vyasa Sai.

energy dissipation components to decrease the antenna quality factor (Q), which results in frequency-selective fading and partly increasing the impedance bandwidth. On the other hand, the traveling wave antenna energy is gradually lost and radiated with transmission, and it is easy to design a larger antenna size and reading area. Therefore, the traveling wave antenna structure is selected as the preferred design in this work.

With regard to UHF RFID NFA design, it is crucial to consider the following three performances, namely, magnetic field distribution, bandwidth and far-field gain [26]. Here, a strong and uniform magnetic field distribution is usually a prerequisite requirement for NFA design, in which the current phase must also be taken into consideration. As there are many standards for UHF RFID, such as the European Telecommunication Standards Institute (ETSI) and Federal Communication Commission (FCC) standards, it would be an added advantage if the NFA has broadband characteristic that can cover the UHF RFID universal band (840-960 MHz). Lastly, a low far-field gain can reduce interference from metal or objects in the far-field for some applications.

In this paper, an NFA with multi-loop structure is proposed. Each loop structure is a double-sided printed $\lambda/2$ loop that can exhibit co-directional current distribution and extendable reading range. In addition to that, lumped resistances are embedded into antenna that greatly reduces the antenna Q value. Because of the above design features, the proposed NFA can demonstrate both strong and uniform magnetic field distribution and broadband characteristic. Notably, this reported work is an extended version of the one reported in [27], in which our modified version has shown better impedance matching (VSWR 1.5 or return loss $\geq$14 dB) across the desired Universal UHF RFID band (840-960 MHz), and we have explicitly explained the design process and methodology. In addition to that, extensive parametric studies are also carried out to explore the operating mechanism of the proposed NFA, which provide useful information for antenna optimization.

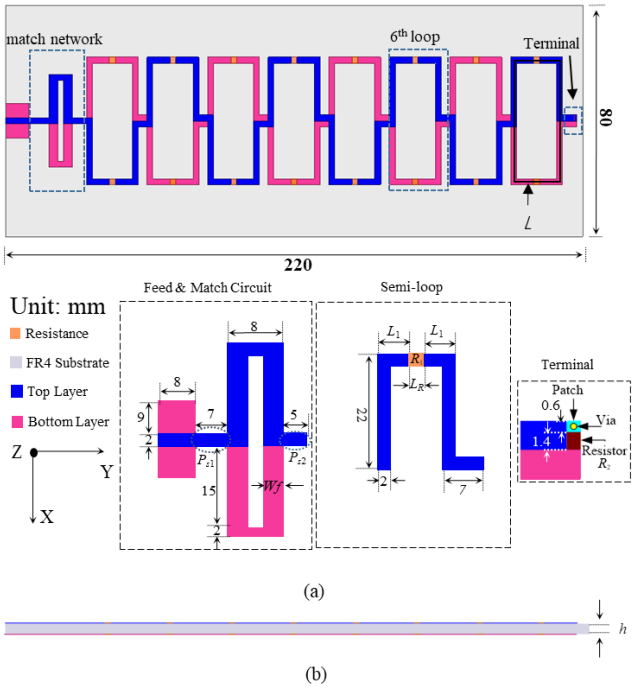

FIGURE 1. Geometry of proposed NFA structure: (a) top view, (b) side view.

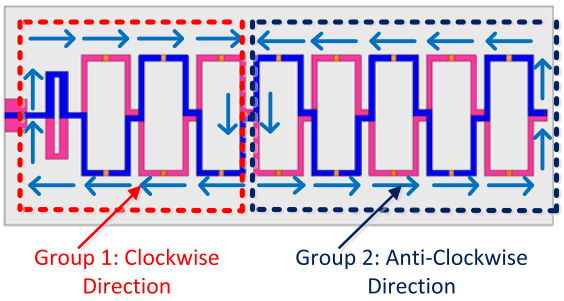

FIGURE 2. Schematic diagram of proposed NFA that can excite two different groups of current flows.

II. ANTENNA CONFIGURATION AND DISCUSSION

The top and side views of the proposed NFA with multi-loop structure are shown in Figs. 1(a) and (b), respectively. It is composed of a small ground (220 mm $\times$ 80 mm), feeding line, narrow-loop matching circuit (match network) [4] and eight rectangular loop structures, and they are printed on both sides (top and bottom) of a 1 mm thick FR4 substrate (relative permittivity of 4.4 and loss tangent of 0.02). Each rectangular loop is formed by incorporating two semi-loops, in which one of them is printed on the top side of the FR4, whereas the other one is printed on the bottom side. Therefore, the magnetic field is reinforced inside the loop, which is defined as the interrogation zone of the antenna. The detailed configuration of the semi-loop is also shown in Fig. 1, and because the overall dimension of the semi-loop is approximately $\lambda/4$, the perimeter of each rectangular loop is approximately $\lambda/2$. Here, each semi-loop is embedded with a lumped resistor ($R_1 = 4.7\ \Omega$), and thus each rectangular loop will be loaded by two lumped resistors R_1. A different lumped resistor ($R_2 = 10\ \Omega$) is soldered at the terminal of the NFA, connecting the top and bottom printed series semi-loops together. The reason for applying these lumped resistors is to decrease the Q value, so that the impedance bandwidth of the proposed NFA can be improved. Even though these lump resistors will also incur a reduction in gain and radiation efficiency (20% at 915 MHz), at the same time, they can avoid the interferences from the far-field unwanted tags and nearby metal when undergoing normal near-field operation of the proposed NFA. Details of these lumped resistances will be further analyzed and discussed in Section III.

Fig. 3 shows the equivalent circuit of the proposed NFA as depicted in Fig. 1. For brevity, the equivalent circuit of the match network is not included. As shown in Fig. 3, because there are 8 loops connected in parallel to each other,

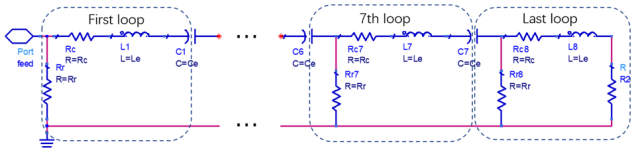

FIGURE 3. Equivalent circuit of proposed NFA.

TABLE 1. The detailed parameters of the proposed NFA.

L_R	L_1	W_f	R_1	R_2
2 mm	9.25 mm	3 mm	4.7 Ω	10 Ω

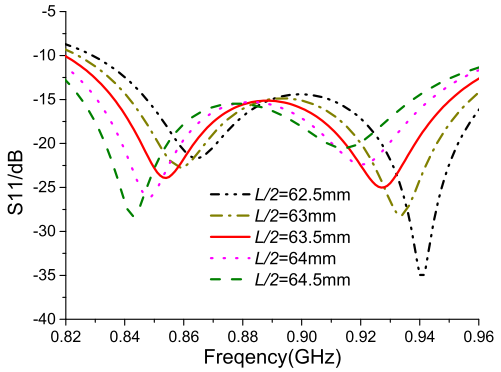

FIGURE 4. The S_{11} responses for different $L/2$.

for simplicity, we only show the equivalent circuit of first loop, partial of 6th loop, 7th loop and last loop (8th loop). Here, each loop can induce an equivalent loop inductor L, in which $L1$ and $L7$ refers to loop inductor 1 and loop inductor 7, respectively. Through energy analysis, the energy loss of the proposed NFA is mainly divided into two parts, namely, the thermal loss (represented by Rc, including dielectric loss and resistance loss) and the radiation loss (represented by Rr), in which Rc7 and Rr7 are referring to the thermal loss and radiation loss, respectively, incurred at the 7th loop. Lastly, due to the coupled energy between two loops, it is analogous to an equivalent capacitor Ci, where i is an integer number (from 1 to 7) referring to the coupling equivalent capacitor between two parallel loops. For example, $C6$ is referring to the coupling equivalent capacitor that incurs between the 6th loop (right side of the longer loop) and 7th loop (left side of the longer loop), and $C7$ refers to the coupling equivalent capacitor incurred between the 7th loop and last loop.

By further observing Figs. 1 and 2, the number of rectangular loop structure adopted in the proposed NFA is eight, and the main reason for that is the 8th loop and matching stub can form two current distribution groups (of different direction, clockwise and anti-clockwise), in which the current flow observed on the loop of either group will be kept in the same direction. Meaning that the current direction of each group is the same, and therefore two independent and equal magnetically readable regions are formed. Because of that, this magnetic field distribution could bring unique advantages/applications for sensitive products (such as biological or pharmaceutical products) that require precise location/position tracking. In addition, the two out-phase current areas can bring large phase difference in the back scatter tag signals between two areas, which is useful for the users to distinguish the location or specific area of a certain product. Notably, the number of rectangular loop structures to be chosen for different NFS is dependent on the required interrogation range. The default parameters of the proposed NFA in Fig. 1 are shown in Table. I.

III. PERFORMANCES STUDIES AND ANALYSIS

Performances studies are carried out in this section to explore the operating mechanism and detail optimization information of the proposed NFA. Magnetic field distribution with different inserted lumped resistors R_1 and R_2 are presented to discuss the resistance selection. Since the RFID tags are usually parallel to the reader, more energy can be stored with stronger vertical magnetic field intensity. Here, the z-component (H_z) magnetic field distributions and other simulated results were performed via ANSYS HFSS 13 software.

In this work, the two types of resistors (R_1 and R_2) employed in this structure are working as energy dissipation components, and thus they are less sensitive with respect to the resonant frequencies. Notably, the resonant frequencies are greatly affected by the rectangular loop perimeter and thickness. To clearly analyze the resonance mechanism, the antenna model with theoretical current distribution scheme has been shown in Figure. 2, and ideally, the current on the outer loop of the antenna is in phase.

A. RECTANGULAR LOOP PERIMETER L

In order to keep the current flowing in a single direction, each rectangular loop structure perimeter is required to be less than λ/2. By setting L as the perimeter, parametric studies are carried out by tuning 1/2 the perimeter ($L/2$) of the rectangular loop, which varies from 64.5 mm to 62.5 mm with a step decrement of 0.5 mm, as shown in Fig. 4. Notably, the variations of this $L/2$ are realized by tuning parameter L_1 from 9.75 mm to 8.75 mm (with step decrement of 0.25 mm). Here, the lumped resistor R_1 is removed from the antenna (thus the length of R_1, now known as L_R, is not included), and by tuning L_1, the entire $L/2$ will also be altered, which can be expressed by the following equation (1):

$$L/2 = 2L_1 + 45 \text{ (mm)} \tag{1}$$

In Eq. (1), the fixed value 45 mm is the fixed combined lengths of the two longer sides of the semi-loop and the length of the stub, ignoring the two lengths L_1 and L_R, as shown in Fig. 1(b). As shown in the bottom figure of Fig. 1(a), $L/2$ is the irregular semi-loop length excluding L_R. When calculating the total length of the semi-loop, we would recommend tuning only L_1, based on Eq. (1). For example, the optimum L_1 in this case is 9.25 mm, thus applying Eq. (1) will yield an optimum $L/2 = 63.5$ mm. Fig. 4 shows the reflection

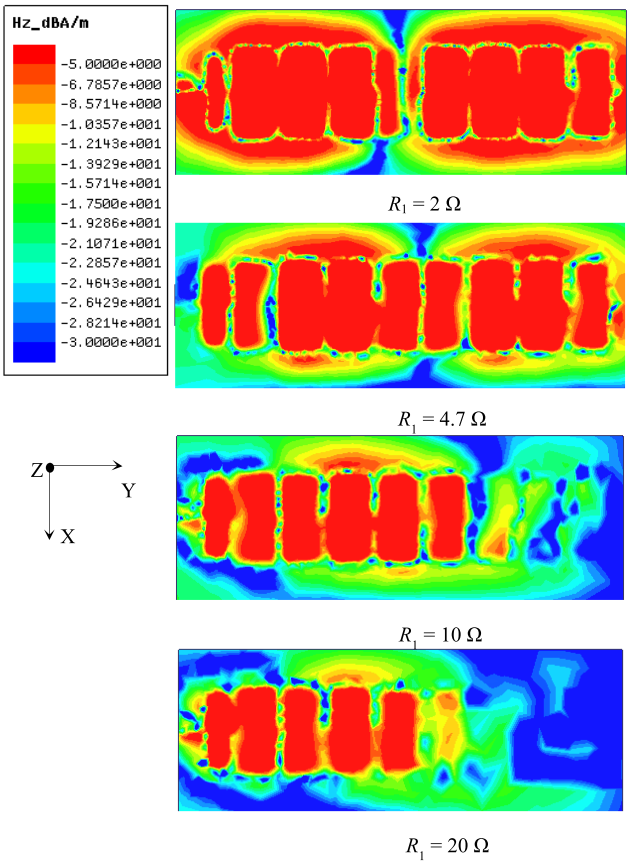

FIGURE 5. Simulated *Hz* for different R1 at z = 0.5 cm, when R2 is fixed at 10 Ω and input power is 30 dBm.

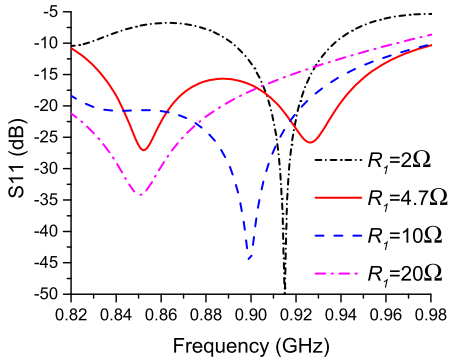

FIGURE 6. Simulated S11 for different R_1, when R_2 is fixed at 10 Ω.

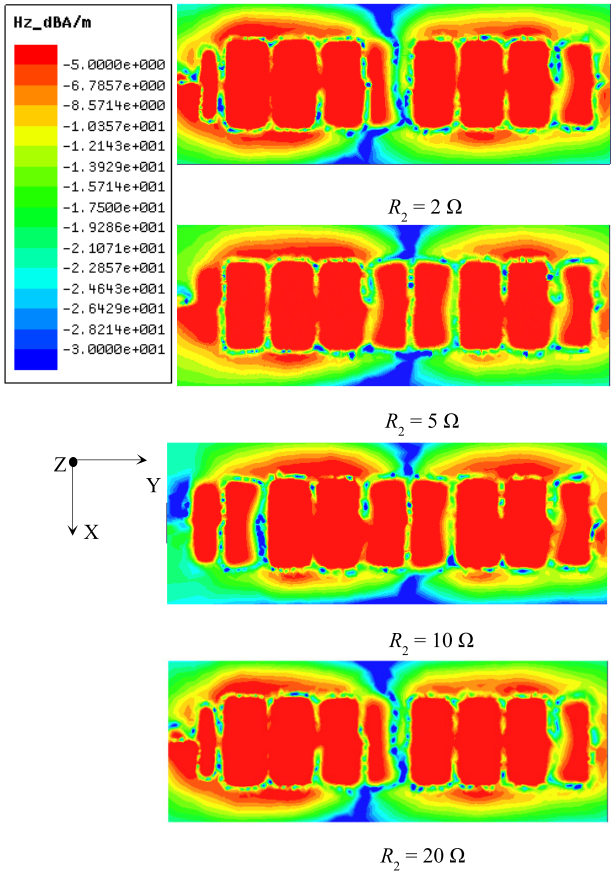

FIGURE 7. Simulated H_z for different R_2 at z = 0.5 cm, when R_1 is fixed at 4.7 Ω and input power is 30dBm.

coefficient (S_{11}) responses for different $L/2$ as aforementioned. Here, it is obvious that decreasing $L/2$ (varying only L_1) will results in linear shifting of the resonant frequency to the higher band (from 850 MHz to 968 MHz), because of the reduced electrical length of the loop structure. Other measures to expand the bandwidth will be discussed later.

B. THE EFFECTS OF RESISTORS R1 AND R2

The two resistors play a significant role in increasing the impedance bandwidth of the propose NFA. As the resistances of these resistors loaded in the antenna structure will greatly affect the input impedance, the matching circuit needs to be adjusted to compensate the impedance variation.

Figure 5 plots the simulated z-oriented magnetic field (H_Z) distribution in the near field for a set of $R_1 = \{2\ \Omega, 4.7\ \Omega, 10\ \Omega, 20\ \Omega\}$ while R_2 is fixed at 10 Ω and the distance from the NFA is 0.5 cm. It is also noteworthy that the simulated input power is set to 30 dBm. In this figure, it can be observed that most of the energy is assumed under the condition that $R_1 = 10\ \Omega$ or 20 Ω, and the magnetic field intensity attenuates dramatically with currents propagation. Fig. 6 shows their corresponding S_{11} curves. Even though the total size of the antenna has far exceeded the desired wavelength for UHF RFID band, one can see that single or dual resonant modes can be excited by the antenna for different R_1. For the case when $R_1 = 4.7\ \Omega$, two resonant modes at near 850 MHz and 925 MHz are excited, and their combined operating band (at VSWR 1.5) can cover the Universal UHF RFID band. Notably, considering the effect on magnetic field and impedance bandwidth, it is obvious that further increasing R_1 will shift the two modes to the lower frequency, while its corresponding magnetic field will also decay. It is noteworthy that the loss of the resistors occupies a certain proportion of the total energy, and as such when $R_1 = 4.7\ \Omega$, the energy loss of the resistor accounting for approximately 20% to 25% of the total energy loss, which is less than the dielectric loss.

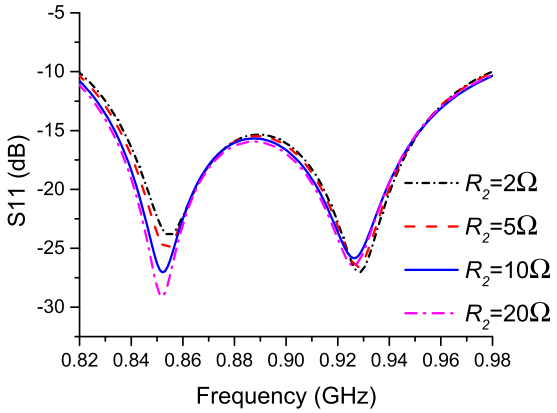

FIGURE 8. Simulated S_{11} for different R_2, when R_1 is fixed at 4.7 Ω.

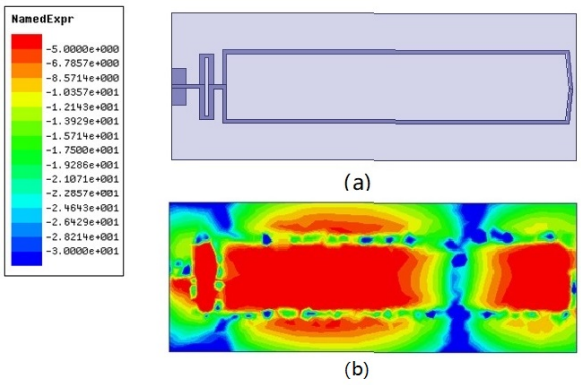

FIGURE 9. The magnetic field distribution of conventional loop antenna.

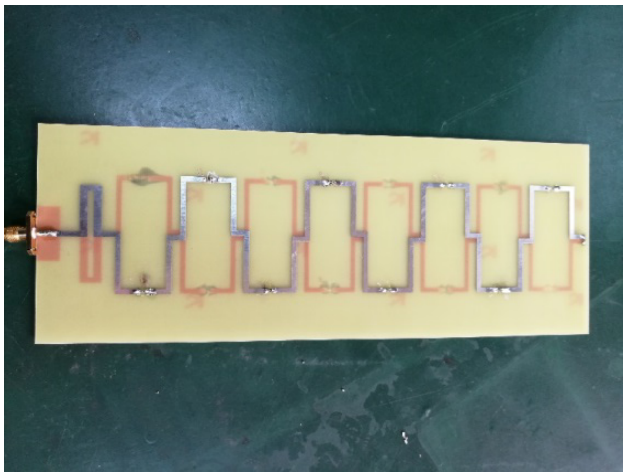

FIGURE 10. The photograph of fabricated antenna.

Fig. 7 plots the simulated z-oriented magnetic field (H_Z) distribution in the near field for a set of $R_2 = \{2\ \Omega, 5\ \Omega, 10\ \Omega, 20\ \Omega\}$ under the condition when R_1 is fixed at 4.7 Ω, and the distance from the NFA is 0.5 cm. Its corresponding simulated S_{11} curves are plotted and shown in Fig. 8. By observing both figures, one can see that the magnetic field strength and impedance bandwidth are only slightly influenced when tuning R_2. The main for that is because R_2 is located at the end of the entire traveling wave antenna (analogous to the general traveling wave antenna characteristics), whereby the heat loss and radiation during the transmission are large, and as such the remaining energy is less than 10% when transmitted to R_2. Therefore, the reflection or absorption of this remaining energy by R_2 will have very little effect on the performances of the antenna. Based on the above studies, the optimized values for R_1 and R_2 in this work are 4.7 Ω and 10 Ω, respectively.

C. THE FEED NETWORK PARAMETERS

In this design, the feed network is applied to work as an impedance matching function, thus the size of feed network will have major impact on the input impedance of the proposed NFA. Specifically, the line width W_f (see Fig. 1(a)) has a great impact on the input impedance, whereas very little impact is seen when tuning the lengths of the paired strip (P_{s1} and P_{s2}). Even though modify/tuning the feed network parameters can significantly affect the input impedance of the proposed NFA, its effect on the antenna's magnetic field distribution is very small. Thus the results of these parametric studies are not shown in detail in the paper.

D. PERFORMANCE COMPARISON WITH CONVENTIONAL LOOP ANTENNA

Fig. 9(a) shows the conventional loop antenna model which has the same size with the proposed antenna. Fig. 9(b) shows the magnetic field distribution of Fig. 9(a) at z = 0.5 cm. It can be seen from Fig. 7 that the uniformity of the magnetic field distribution of the proposed antenna is obviously better than Fig. 9(b). The magnetic field of the conventional antenna is split in three pieces, because it is now a standing wave antenna, and the current node point and the magnetic field split point are fix. It can be seen that the ''null reading regions (dark blue region)'' are very obvious even at a short distance. From the perspective of impedance characteristics, the traditional antenna is a standing wave antenna, and the bandwidth is very narrow. In summary, compared with the proposed antenna, the performance of the conventional antenna is worse in terms of magnetic field distribution and impedance bandwidth.

IV. ANTENNA PERFORMANCES

The proposed NFA was fabricated, and its corresponding photograph is shown in Fig. 10. In this section, typical near-field antenna performances such as bandwidth, magnetic field distribution, far-field gain and reading range are investigated and presented.

A. IMPEDANCE BANDWIDTH AND IMPEDANCE MATCHING

The measured and simulated S_{11} of the proposed NFA are shown in Fig. 11, and the two results agree well with each

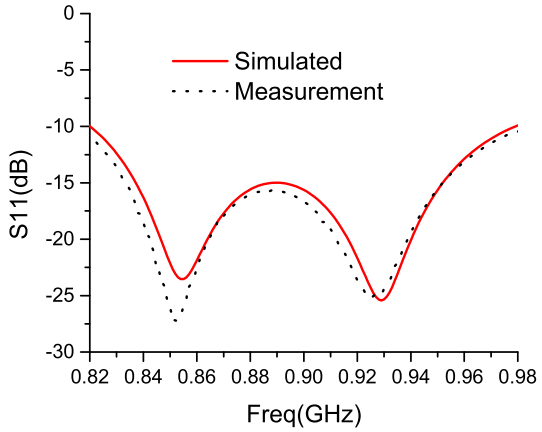

FIGURE 11. The simulated and measured S_{11} of proposed NFA.

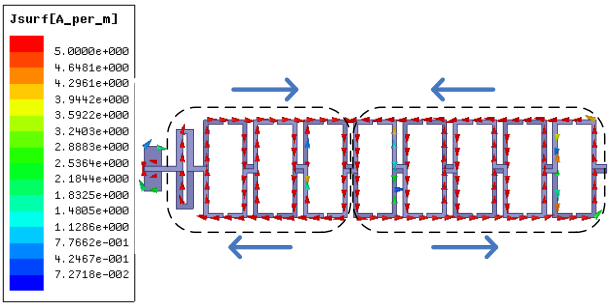

FIGURE 12. Simulated current distribution of proposed NFA.

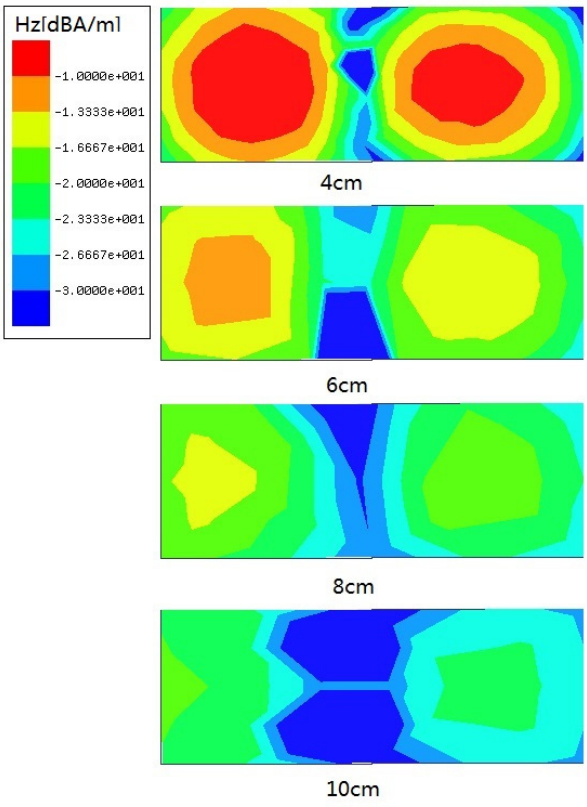

FIGURE 13. The magnetic field (H_z) distribution at 915 MHz.

other. Here, the measured 10-dB impedance bandwidth was approximately 18.7% (816-984 MHz), which can cover both FCC and ETSI standards. If a much stringent standard is required, the proposed NFA can still satisfied the Universal UHF RFID band requirement because the measured 1.5 VSWR or 14-dB return loss was 13.8% (831-955 MHz).

B. CURRENT, MAGNETIC DISTRIBUTION AND GAIN

Figure 12 shows the simulated current distribution of the proposed NFA. The current distribution of the antenna is obviously the same as the result of the analysis in Fig. 2. Evidently, the currents in each rectangular loop (for the two groups rotating in different direction, as shown in Fig. 2) are kept in a single direction, which strengthen the magnetic field intensity inside the central region of these two groups of the NFA. The current causes the antenna to produce two stable reading areas, which can be confirmed by the magnetic field distribution.

Figure 13 shows the simulated transient H_z distribution at 915 MHz for different vertical heights (along the z-axis), which are 4 cm, 6 cm, 8 cm, and 10 cm. Obviously, the field intensity will decay linearly with increasing height, but there are two tag readable areas (contributed by the magnetic field intensity inside the central region of these two groups of the NFA). Fig. 14 shows the simulated H_z distributions at 865 MHz in the same heights as Fig. 13. Similar conclusions as those at 915 MHz can be drawn. But at 868 MHz, the magnetic field strength of the two readable regions of the antenna is more balanced at higher heights. Here, because the far-field gain of the antenna is lower than 1 dB, and the radiation (beam direction) of the proposed NFA is parallel to the antenna plane and vertical to the direction of reading the tag, this radiation pattern ensures that the proposed NFA is less susceptible to interference from the far-field.

C. READING PERFORMANCES

To further verify the reading performances of the proposed NFA, measurement experiments are carried out. Fig. 15 shows the measurement configuration, in which the experiment system is composed of three major parts, namely, reader system (including the proposed NFA), post-processing system and RFID tag. Here, the reader system applied is an Impinj Indy R2000 reader with 30 dBm output power at ETSI and FCC bands. Before conducting the experiment, the proposed NFA surface is subdivided into 5 $\times$ 12 intersections, and the size of each grid is 20 mm $\times$ 20 mm. The RFID tag used in this experiment is a commercial J41 Impinj near-field tag (of diameter 12 mm) with working frequency of 860-960 MHz. The read sensitivity of this J41 tag is -20 dBm, and the tag chip (of J41) used in the experiment is Impinj Monza 4. The tag will be placed on each intersection of the grid, and the detection measurements are repeated in each intersection through changing the position of the tag.

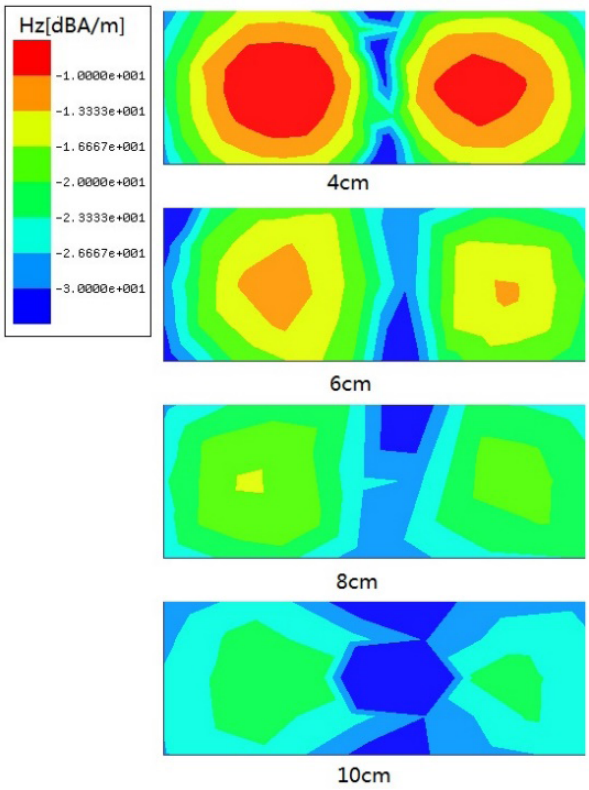

FIGURE 14. The magnetic field (H_z) distribution at 865 MHz.

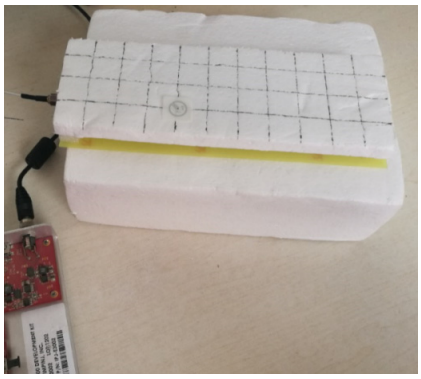

FIGURE 15. The measurement configuration.

Notably, as of whether the tag is correctly detected or not, the measured results are recorded by post-processing system.

Figure 16 shows the measurement results when the RFID tag is positioned above the proposed NFA via a styrofoam board of 3 different thicknesses (6 cm, 8 cm, and 10 cm). At 4 cm reading range, the tag can be successfully read by the proposed NFA (via all the grids), however, when it is positioned at 6 cm, only two grids are not detected. For the case when the reading ranges are 8 cm and 10 cm, it is obvious that the effective reading areas (or detection regions) are mostly concentrated at the two center regions, which coincide with the simulations denoted in Figs. 13 and 14. Fig. 17 shows the measured readable tag number at different heights.

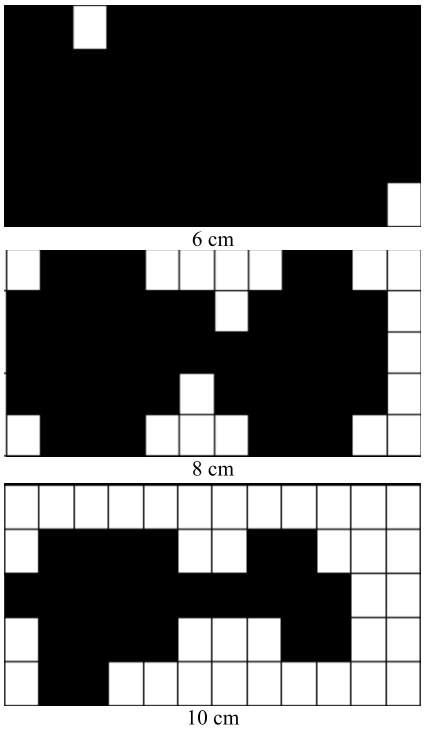

FIGURE 16. Measured reading area at different distances above the antenna surface.

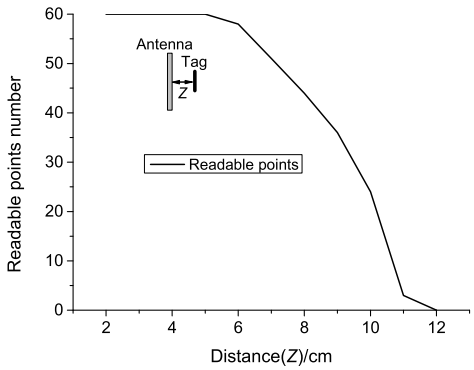

FIGURE 17. Readable points versus reading range.

TABLE 2. Antenna performance comparison between the proposed NFA and references.

Reference	Size (mm)	10-dB Bandwidth	Read range (cm)	Full range read distance (mm)
[6]	150×150	13.3%	10	50
[17]	200×200	3.2%	10	-
[21]	833×80	>20%	5	Less than 30
[25]	776×120	9.36%	6.5	12
[28]	480×200	1.6%	6.5	20
Proposed	220×80	18.7%	11	50

By observing the above results, one can see that the proposed NFA is suitable for large interrogation area applications such as RFID book shelve application etc. Table 2 lists the performance comparisons of other antennas reported in

recent years and the proposed NFA. The experiment powers applied by these antennas are 30 dBm. In Table 2, besides exhibiting broader impedance bandwidth, one can see that the proposed NFA has also demonstrated better reading ranges due to strong magnetic field. Notably, the advantage of longer reading range is also due to a relatively large electrical size, but when comparing the proposed NFA to [17], [21] and [25]; it has smaller planar size (area) than them. Here, [28] has a very large access area of 480 mm $\times$ 220 mm, which is suitable for wide range RFID applications. However, because the antenna energy is more dispersed, the full range read distance and the maximum reading distance are both worse than the proposed NFA. In addition, the bandwidth of [28] is only 15 MHz that cannot cover the FCC (26 MHz) band. As for [29], it has a very large reading area of 440 mm $\times$ 160 mm, and has used 17 dBm input power and therefore not suitable to be included and compared with the other reference antennas in Table 2 (as all reference antennas in Table 2 are using 30 dBm input power). Even though [29] was fed by a lower input power and has exhibited a maximum read range of 14 cm, while most of the tags (reading rate $>$95%) are successfully read at 10 mm, the full range read distance of [29] was too short or does not exist. In addition, the operation band of [29] was 880-980 MHz that cannot cover the ETSI band (865-868 MHz).

V. CONCLUSON

A multi-loop near-field antenna for UHF RFID application is successfully proposed and investigated. It has an overall size of 220 m $\times$80 mm $\times$ 1 mm. The proposed NFA is composed of eight $\lambda/2$ combined rectangular loops printed on the upper and lower FR4 substrate surfaces, which is an extendable structure that can ensure a strong and uniform magnetic field distribution. To obtain broad 10-dB impedance bandwidth of up to 18.7% (816-984 MHz) for covering both ETSI and FCC bands, two types of resistors are loaded into the proposed NFA to decrease the Q value. It is also noteworthy that the impedance bandwidth (at VSWR 1.5) of the proposed NFA can also cover the Universal UHF RFID band. The proposed NFA can achieve 100% reading rate at optimum reading range of 5 cm.

REFERENCES

[1] V. Chawla and D. Ha, "An overview of passive RFID," *IEEE Commun. Mag.*, vol. 45, no. 9, pp. 11–17, Sep. 2007.
[2] A. Michel, A. Buffi, R. Caso, P. Nepa, G. Isola, and H. T. Chou, "Design and performance analysis of a planar antenna for near-field UHF-RFID desktop readers," in *Proc. Asia–Pacific Microw. Conf. Proc.*, Dec. 2012, pp. 1019–1021.
[3] Z. Xing, L. Wang, C. Wu, and K. Wei, "Study of broadband near-field antenna for ultra-high-frequency radio frequency identification applications," *IET Microw., Antennas Propag.*, vol. 5, no. 14, pp. 1661–1669, Nov. 2011.
[4] X. Qing, C. K. Goh, and Z. N. Chen, "A broadband near-field UHF RFID antenna," *IEEE Trans. Antennas Propag.*, vol. 58, no. 12, pp. 3829–3838, Dec. 2010.
[5] X. Li, J. Liao, Y. Yuan, and D. Yu, "Segmented coupling eye-shape UHF band near field antenna design," in *Proc. Asia–Pacific Microw. Conf.*, Dec. 2009, pp. 2401–2404.
[6] J. Kizhekke Pakkathillam and M. Kanagasabai, "A novel UHF near-field RFID reader antenna deploying CSRR elements," *IEEE Trans. Antennas Propag.*, vol. 65, no. 4, pp. 2047–2050, Apr. 2017.
[7] B. Shrestha, A. Elsherbeni, and L. Ukkonen, "UHF RFID reader antenna for near-field and far-field operations," *IEEE Antennas Wireless Propag. Lett.*, vol. 10, pp. 1274–1277, 2011.
[8] D. Ding, J. Xia, L. Yang, and X. Ding, "Multiobjective optimization design for electrically large coverage: Fragment-type near-fieldfar-field UHF RFID reader antenna design," *IEEE Antennas Propag. Mag.*, vol. 60, no. 1, pp. 27–37, Feb. 2018.
[9] Y. Sim Ong, X. Qing, C. Khan Goh, and Z. Ning Chen, "A segmented loop antenna for UHF near-field RFID," in *Proc. IEEE Antennas Propag. Soc. Int. Symp.*, Jul. 2010, pp. 1–4.
[10] X. Li and L. Cao, "Microstrip-based segmented coupling reader antenna for near-field UHF RFID applications," *Microw. Opt. Technol. Lett.*, vol. 53, no. 8, pp. 1774–1777, Aug. 2011.
[11] J. Shi, X. Qing, and Z. N. Chen, "Electrically large zero-phase-shift line grid-array UHF near-field RFID reader antenna," *IEEE Trans. Antennas Propag.*, vol. 62, no. 4, pp. 2201–2208, Apr. 2014.
[12] D. M. Dobkin, S. M. Weigand, and N. Iyec, "Segmented magnetic antennas for near-field UHF RFID," *Microw. J.*, vol. 50, no. 6, pp. 96–102, Jun. 2007.
[13] Z. N. Chen, C. K. Goh, and X. Qing, "Loop antenna for UHF near-field RFID reader," in *Proc. 4th Eur. Conf. Antenna Propag.*, Apr. 2010, pp. 1–4.
[14] X.-D. Wei, H.-L. Zhang, and B.-J. Hu, "Novel broadband center-fed UHF near-field RFID reader antenna," *IEEE Antennas Wireless Propag. Lett.*, vol. 14, pp. 703–706, 2015.
[15] X.-D. Wei, B.-J. Hu, and H.-L. Zhang, "Novel UHF near-field RFID reader antenna based on double-sided parallel-strip line," *IEEE Antennas Wireless Propag. Lett.*, vol. 13, pp. 419–422, 2014.
[16] C. Cho, J. Ryoo, I. Park, and H. Choo, "Design of a novel ultra-high frequency radio-frequency identification reader antenna for near-field communications using oppositely directed currents," *IET Microw., Antennas Propag.*, vol. 4, no. 10, pp. 1543–1548, Oct. 2010.
[17] C. Cho, C. Lee, J. Ryoo, and H. Choo, "Planar near-field RFID reader antenna for item-level tagging," *IEEE Antennas Wireless Propag. Lett.*, vol. 10, pp. 1100–1103, 2011.
[18] L. Shen, H. Xiang, W. Tang, W. Zhuang, and J. Ma, "An end-fire dipole array for big interrogation zone of near-field RFID," in *Proc. IEEE Int. Symp. Antennas Propag. USNC/URSI Nat. Radio Sci. Meeting*, Jul. 2015, pp. 1582–1583.
[19] L. Shen, W. Tang, H. Xiang, and W. Zhuang, "A novel antenna achieving null-less magnetic field distribution for near-field UHF RFID," in *Proc. Int. Symp. Antennas Propag. Conf. Proc.*, Dec. 2014, pp. 547–548.
[20] A. Michel and P. Nepa, "UHF-RFID desktop reader antennas: Performance analysis in the near-field region," *IEEE Antennas Wireless Propag. Lett.*, vol. 15, pp. 1430–1433, 2016.
[21] A. Ren, C. Wu, Y. Gao, and Y. Yuan, "A robust UHF near-field RFID reader antenna," *IEEE Trans. Antennas Propag.*, vol. 60, no. 4, pp. 1690–1697, Apr. 2012.
[22] A. Michel, A. Buffi, P. Nepa, R. Caso, and G. Isola, "Meandered TWAs array for near-field UHF RFID applications," *Electron. Lett.*, vol. 50, no. 1, pp. 17–18, Jan. 2014.
[23] A. Michel, R. Caso, A. Buffi, P. Nepa, and G. Isola, "An array of meander travelling wave antennas for near-field UHF-RFID readers," in *Proc. IEEE Antennas Propag. Soc. Int. Symp. (APSURSI)*, Jul. 2013, pp. 1732–1733.
[24] R. Caso, A. Michel, A. Buffi, P. Nepa, and G. Isola, "A modular antenna for UHF RFID near-field desktop reader," in *Proc. IEEE RFID Technol. Appl. Conf. (RFID-TA)*, Sep. 2014, pp. 204–207.
[25] Y. Yao, Y. Liang, J. Yu, and X. Chen, "A broadband near-field UHF RFID reader antenna with low far-field gain," *IEEE Trans. Antennas Propag.*, vol. 65, no. 9, pp. 4869–4874, Sep. 2017.
[26] P. Nikitin, K. V. S. Rao, and S. Lazar, "An overview of near field UHF RFID," in *Proc. IEEE Int. Conf. RFID*, Mar. 2007, pp. 167–174.
[27] H. Li and Z. Xing, "A long chain-like reader antenna for UHF RFID application," in *Proc. 6th Asia–Pacific Conf. Antennas Propag. (APCAP)*, Oct. 2017, pp. 1–2.
[28] Y. Yao, C. Cui, J. Yu, and X. Chen, "A meander line UHF RFID reader antenna for near-field applications," *IEEE Trans. Antennas Propag.*, vol. 65, no. 1, pp. 82–91, Jan. 2017.
[29] L. Shen, C. Huang, C. Wang, W. Tang, W. Zhuang, J. Xu, and Q. Ding, "A Yagi–Uda antenna with load and additional reflector for near-field UHF RFID," *IEEE Antennas Wireless Propag. Lett.*, vol. 16, pp. 728–731, 2017.

ZIJIAN XING was born in Gansu, China, in November 1985. He received the B.Eng., M.Eng., and Ph.D. degrees from Northwestern Polytechnical University, China, in 2008, 2011, and 2014, respectively. From 2014 to 2018, he worked as an Assistant Professor with Northwestern Polytechnical University, where he became an Associate Professor, in July 2018. He has published over ten SCI research articles. He was the Principal Investigator of three scientific research projects of antennas, including the National Natural Science Foundation of China. His research interests include circularly polarized antenna arrays, radio frequency identification circuits, and near-field antenna technology. He also serves as a Reviewer for all the IEEE and IET journals related to antennas.

HAOTIAN LI was born in Shifang, China, in 1995. He received the B.Eng. degree in electromagnetics and wireless technology from Northwestern Polytechnical University (NPU), Xi'an, China, in 2017. He is currently pursuing the Ph.D. degree in electromagnetics and microwave technology with the University of Electronic Science and Technology of China (UESTC), Chengdu, China.

His current research interests include time modulation techniques in antenna arrays, phased arrays, and antennas for RFID applications.

CHOW-YEN-DESMOND SIM (Senior Member, IEEE) was born in Singapore, in 1971. He received the B.Sc. degree from the Department of Engineering, University of Leicester, U.K., in 1998, and the Ph.D. degree from the Department of Engineering, Radio System Group, University of Leicester, in 2003. From 2003 to 2007, he was an Assistant Professor with the Department of Computer and Communication Engineering, Chienkuo Technology University, Changhua, Taiwan. In 2007, he joined the Department of Electrical Engineering, Feng Chia University (FCU), Taichung, Taiwan, as an Associate Professor, where he became a Full Professor, in 2012, and a Distinguish Professor, in 2017. He has served as the Executive Officer of the master's degree with the College of Information and Electrical Engineering (industrial research and development) and the Director of intelligent industrial IoT Ph.D. degree, from August 2015 to July 2018. He is currently serving as the Head of the Department of Electrical Engineering and the Director of the Antennas and Microwave Circuits Innovation Research Center, Feng Chia University. He has authored or coauthored over 130 SCI articles. His current research interests include antenna design, VHF/UHF tropospheric propagation, and RFID applications. He is a Fellow of the Institute of Engineering and Technology (FIET), a Senior Member of the IEEE Antennas and Propagation Society, and a Life Member of the IAET. He served as the TPC Member of the APMC 2012, the APCAP 2015, IMWS-Bio 2015, CSQRWC 2016, ICCEM 2017, APCAP 2018, CIAP 2018, and APMC 2019. He was invited as the Workshop/Tutorial Speaker of APEMC 2015, iAIM 2017, and InCAP 2018, and an Invited Speaker of TDAT 2015, iWAT 2018, APCAP 2018, ISAP 2019, and InCAP 2019. He was the Keynote Speaker of the IEEE SOLI 2018. Since October 2016, he has been serving as the Technical Consultant of Securitag Assembly Group (SAG), which is one of the largest RFID tag manufacturers in Taiwan. He was the recipient of the IEEE Antennas and Propagation Society Outstanding Reviewer Award for the IEEE TRANSACTIONS ANTENNAS AND PROPAGATION, from 2014 to 2019, for six consecutive years. He has also received the Outstanding Associate Editor Award for the IEEE ANTENNAS WIRELESS AND PROPAGATION LETTERS, in July 2018. He has also served as the TPC Sub-Committee Chair (Antenna) of the ISAP 2014, PIERS 2017, and PIERS 2019. He has served on the Advisory Committee of InCAP 2018/2019 and has also served as the TPC Chair of the APCAP 2016 and iWEM 2019. He has served as the Chapter Chair of the IEEE AP-Society, Taipei Chapter, from 2016 to 2017, and he has been the founding Chapter Chair of the IEEE Council of RFID, Taipei Chapter, since 2017. He is currently serving as an Associate Editor for the IEEE ANTENNAS AND WIRELESS PROPAGATION LETTERS, IEEE ACCESS, the IEEE JOURNAL OF RADIO FREQUENCY IDENTIFICATION, and the *International Journal of RF and Microwave Computer-Aided Engineering* (Wiley).

JIANYING LI received the B.Sc. degree in mathematics from Henan Normal University, Xinxiang, China, in 1986, and the M.Eng.Sc. and Ph.D. degrees in electromagnetic field and microwave technology from Xidian University, Xi'an, China, in 1992 and 1999, respectively. From 1992 to 1996, he was with the Xi'an Electronic Engineering Research Institute, Xi'an, as a Research Engineer. From 1999 to 2004, he was with the Department of Electrical and Computer Engineering, National University of Singapore (NUS). He was a Postdoctoral Research Fellow and then a High Performance Computation for Engineered Systems (HPCES) Programmer with Singapore-MIT Alliance (SMA). From 2005 to 2010, he was with the Temasek Laboratories, NUS, where he was a Research Scientist. Since 2011, he has been with the School of Electronics and Information Engineering, Northwestern Polytechnical University. His current research interests include fast algorithms and its applications to radar cross-sections, the analysis and design of phased arrays, waveguide slot antennas, and microstrip antennas, and EM periodic structures.

ZILIANG LI received the B.Sc. degree in electronic science and technology from the North China University of Water Resources and Electric Power, Zhengzhou, China, in 2019. He is currently pursuing the master's degree in electromagnetic field and microwave technology with Northwestern Polytechnical University, Xi'an, China. His recent research interests include microstrip antennas and circularly-polarized antennas.